J. Electroanal. Chem., 168 (1984) 335—354
Elsevier Sequoia S.A., Lausanne — Printed in The Netherlands

ANALYSIS OF IMPEDANCE DATA FOR SINGLE CRYSTAL Na β-ALUMINA AT LOW TEMPERATURES

J. R. MACDONALD and G. B. COOK
Department of Physics and Astronomy, University of North Carolina, Chapel Hill, North Carolina 27514 (USA)

ABSTRACT

A detailed re-analysis of the 83-151 K impedance-frequency data of Bruce *et al.* on Na β-alumina has been carried out using complex least-squares fitting of the data to a circuit which includes two constant phase elements. Three-dimensional plotting of the complex modulus function, $M \equiv M' + iM''$, *vs* the logarithm of the frequency ν is found to show glitches and anomalies in the data not obvious in ordinary spectrographic plots of M' or M'' *vs* log(ν) or in M' and M'' complex-plane plots. In spite of some such anomalies in the data, excellent fits to the circuit model are obtained, especially at the lower temperatures. Surprisingly, all circuit elements seem to be thermally activated, with the activation lines split into two very clearly defined, offset sections for the separate ranges 83 to 102 K and 110 to 151 K. These results suggest, even more strongly than an earlier more approximate analysis of the same data by Ngai and Strom, the presence of a glass-like transition, with Vogel temperature T_∞ falling between 102 and 110 K. This possibility, and the additional possibility of a direct connection between the low-frequency limiting conductivity and the Na-ion hopping rate, are investigated and discussed in detail; some measure of agreement is found between various parameters derived from the present fitting results and those obtained from other types of measurements.

INTRODUCTION

The crystalline material Na β-alumina $[(1 + x)Na_2O \cdot 11Al_2O_3]$ has a large, liquid-like ionic conductivity arising from the motion of high-mobility Na ions at room temperature and above [1] when the material is non-stoichiometric ($x > 0$), but it appears to show glass-like electrical, thermal, and acoustic properties at sufficiently low temperatures [2,3]. This material, a member of the class of superionic conductors or solid electrolytes, has become of great interest in recent years because of its high ionic conductivity and potential applicability as an electrolyte in batteries and fuel cells.

Although there has been much theoretical and experimental work carried out on β-alumina (see the recent review of Strom [3]), there still remains some uncertainty about its detailed conduction mechanism [3,4], and measurements on different single crystals usually yield [1,5-7] somewhat different pre-exponential factors and activation energies for σT, where σ is the effective DC

0022-0728/84/$03.00

conductivity. Because of the usual excess of Na ions in single crystals of Na β-alumina over the stoichiometric value ($x = 0$), there must be charge compensating oxygen ions present as well, leading to a high degree of disorder in the c-planes of the material where conduction is greatly favored. It is this disorder which makes the conduction liquid-like and probably results in wide distributions of various physical properties.

Impedance data for Na β-alumina have been gathered for the ranges 25 °C ≤ T ≤ 500 °C [6] and 83 K ≤ T ≤ 151 K [8-10], but no detailed analysis of the data using nonlinear complex least-squares fitting [11] to an equivalent circuit or specific analytic model seems to have been carried out, especially for the interesting low-temperature region where dielectric and glass-like properties appear. For this reason, and because Ngai and Strom [2] have developed evidence for a glass-like transition in Na β-alumina near 120 K, we have felt it worthwile to analyze the 83 - 151 K data of Almond and West [8,9] using both complex least-squares data fitting and three-dimensional (3-D) perspective data plotting techniques [12].

Although part of these low-temperature data, in the form of the imaginary part, M'', of the complex modulus function, M, *vs* frequency, has been compared [2] with the predictions of the fractional-exponential-decay heuristic model of Williams and Watts [13] (and with the more microscopic infrared divergence model of Ngai [14], which yields essentially this same response), the results were necessarily quite approximate (although not so stated). First, because the use of either a real or an imaginary part of a response-function for fitting, instead of using both simultaneously [11], leads to less fitting accuracy, but more importantly, because no closed form of the fractional exponential response function is known (except when its parameter n equals 0, 1/3, 1/2, or 1). Ngai and Strom [2] were unable to employ least-squares fitting to determine all the parameter estimates and were apparently restricted to using n values at 0.025 intervals, possibly obtained from the tables of Moynihan [15].

In the next section, we shall consider the Na β-alumina data and how they may best be presented. Then, we shall discuss least-squares fitting and appropriate weighting, and show fitting results for a plausible equivalent circuit by presenting direct comparison of the original data and predictions obtained from fitting. The parameter estimates obtained from the fitting will be discussed and interpreted in the final section.

DATA AND DATA FITTING RESULTS

Data presentation

Impedance data [8-10] for single-crystal Na β-alumina covering the temperature range of 83 to 151 K and the frequency range from 10^2 to 7×10^6

Hz were kindly supplied by West [16]. The single-crystal material was melt grown at Union Carbide and ionically blocking gold electrodes were employed because ohmic electrodes were impractical in this temperature range. Although the non-stoichiometry fraction x was unstated, it generally falls in the 0.2 to 0.3 region for crystals of this type [3]; we shall use here the value 0.227 determined in [5] and employed by Wang [4].

Although impedances, $Z = Z' + iZ''$, or admittances, $Y \equiv Z^{-1} = Y' + iY''$, are usually directly measured in small-signal AC measurements of the response of conducting/dielectric materials, two derived complex quantities, the complex dielectric constant, $\epsilon \equiv Y/(i\omega C_0) = \epsilon' - i\epsilon''$, and the complex modulus function, $M \equiv \epsilon^{-1} \equiv i\omega C_0 Z = M' + iM''$, have also been employed. Here $\omega \equiv 2\pi\nu$ is the angular frequency; $C_0 \equiv \epsilon_0 A_c/\ell \equiv \epsilon_0/g$ is the vacuum capacitance of the measuring cell; ϵ_0 is the permittivity of free space; and $g \equiv \ell/A_c$ is the cell constant, involving the electrode separation ℓ and the effective electrode area A_c. The complex dielectric constant has often been employed for low-conductivity "dielectric" materials, and Z, Y, or M for high-conductivity materials. It has been suggested [17] that impedance spectroscopy data, in the form of impedance *vs* log frequency, highlights electrode and/or grain boundary effects while M *vs* log(ν) data is useful in emphasizing bulk effects. The use of the modulus function was perhaps first suggested by Schrama [18] in the present context, and it has been widely applied in recent years by Moynihan and his collaborators [15]. Spectroscopic plots of log (-Z'') and log(M'') *vs* log(ν) have been also used by others [8-10] and are particularly appropriate when Z'' or M'' vary over wide ranges.

Starting with the widely employed Argand-diagram, Cole-Cole plot [19] of ϵ'' *vs* ϵ' with frequency usually implicit, complex-plane presentations of Z and Y have been extensively used as well [20-24]. But spectroscopic and complex-plane types of presentation either suppress some of the data or do not show clearly how all parts of the data co-vary. Luckily, three-dimensional perspective plots [12] (e.g., Z', -Z'' and log(ν) or log(Z'), log(-Z'') and log(ν)) combine the approaches and can clearly show all details of the data. Thus, we shall use such plots in the present work. Because Z, Y, M, and ε data representations weight results differently, it is often useful to examine 3-D plots for more than one of these choices.

Figure 1(a) is a 3-D plot of Z^* (we reserve the superscript asterisk to indicate complex conjugation of complex functions) for the raw Na β-alumina data at 83 K. All machine-plotted 3-D plots presented here use solid dots for the data (connected by straight lines) and open dots for the projections in the three planes, i.e., the planes $Im(Z^*)$ *vs* log(ν), $Im(Z^*)$ *vs* $Re(Z^*)$, and $Re(Z^*)$ *vs* log(ν). We shall generally include, as shown, projection lines from the data points to the bottom plane. The log(ν) scale in all the 3-D plots

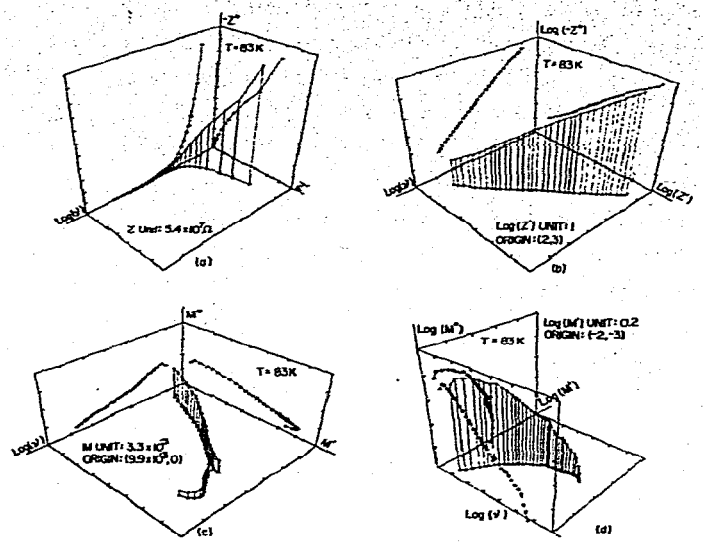

Fig. 1. Three-dimensional plots of the 83 K data: (a) $Z^* = Z' - iZ''$; (b) log(Z'), log(-Z''); (c) M = M' + iM''; and (d) log(M'), log(M'').

always starts at 1, and its scale interval (between tickmarks) will always be 1 (an actual factor of 10). For regular 3-D plots, the zeros of the quantities plotted will be at the origin unless otherwise noted, with scale factors as shown. Finally, for 3-D log plots, the origin values and scale factors (in log space) will be as shown on the plot. As usual, scales for real and imaginary parts of a complex quantity will be taken the same. Figure 1(a) demonstrates several important points. First, a linear presentation can only show one or two orders of magnitude variation clearly; here |Z| varies over more than four decades and much of the data are thus unresolved. Second, the lowest frequency point appears somewhat inconsistent with the nearby higher frequency points. This is obvious from the 3-D curve and from the complex-plane projection curve, but it does not show up at all in the two impedance-spectroscopy plots (in the other two planes) which involve log(ν) directly. If these curves were all that were examined, as is frequently the case, the difficulty in the last data point position would remain unappreciated.

The problem of adequately resolving regions where |Z| is small is solved in large measure by employing a 3-D plot involving log(Z') and log (-Z''), as in Fig. 1(b). We present in Figs. 1(c) and 1(d) a 3-D M-plot and log(M) plot

for the same data. Several new glitches not apparent, or not as apparent, in Figs. 1(a) and 1(b) now appear because of the high frequency emphasis inherent in M. The anomaly associated with the lowest frequency point is again apparent, this time especially in the three projections. We now see an anomalous region near the middle of the data which was hardly apparent in Fig. 1(b). Apparently, overlapping data were taken with two types of measuring apparatuses. Clearly, the results are not very consistent in this region. We have sometimes averaged the common-frequency data values, when present, before fitting, or alternatively, have allowed the least-squares fitting to do the averaging. Incidentally, this 83 K overlap region is the most inaccurate and it renders the final 83 K results somewhat suspect. Finally, Fig. 1(c) shows that the three highest-frequency M' points begin to decrease with frequency. But there is nothing in the usual models of M in terms of a distribution made up of a series combination of many individual parallel resistive and capacitative elements [15] or in the plausible fitting circuit we shall employ that can lead to such a drop off. Therefore, we have usually omitted such points from the fitting for this and the higher temperatures and have thereby improved the degree of fit appreciably.

Data weighting

First we must consider what type of weighting to employ. We have used P-weighting [11] here throughout for the following reasons. This is weighting calculated by assuming that the uncertainty of the real or imaginary part of a complex quantity is proportional to the magnitude of that part. P-weighting is particularly appropriate for the present data which vary in magnitude by several powers of ten for a given temperature as frequency is changed. It is also reasonable physically for most measuring techniques, and it leads to exactly the same parameter estimates and relative residuals for both Z and M fits and for both Y and ϵ fits. Thus, only two separate fits, say Z and Y, need be considered. It may be expected that with random and systematic errors in the data there will always be differences in parameter estimates obtained from separate Z and Y fits. We indeed find such differences. Since Z rather than Y was apparently measured directly here [8-10], we shall derive all parameters from Z fits. We thus avoid possible bias in parameter estimates introduced by the inverse transformation from Z to Y. There is another alternative worth mentioning, however. If M-weighting is used, one generally finds that Z and Y parameter estimates are so close together that one need not distinguish between them. Such weighting, say for Z data, uses weights for both Z' and Z'' residuals derived from the assumption that the errors in both these quantities are proportional to $|Z|$. But $|Z'|$ and $|Z''|$ are often very different in magnitude, yet M-weighting unrealistically weights their

residuals equally, quite unlike P-weighting. On the other hand, when |Z| and Arg(Z) are measured directly, P-weighting involving |Z| and Arg(Z) seems most appropriate.

Fitting circuit

Because of the unavailability of a closed-form expression for the fractional exponential system function (e.g., Z *vs* ν), we elected not to try to fit the data to this model. Previous work [6,8-10,24] suggested that the constant phase element (CPE) could be profitably used as part of the fitting circuit. One interpretation of it involves a possibly wide distribution of relaxation times [25]. Its expression as an admittance is best [26] written as

$$Y_{CPE} = A_0(i\omega)^n \qquad (1)$$

where the parameters A_0 and n are usually temperature dependent. Note that this n(T) is not exactly the same as the n(T) which appears in the fractional exponential (FE) model, although they are closely related since both the FE and the CPE lead to t^{-n} time-dependence over appreciable ranges of time. We shall, therefore, compare the approximate n(T) results obtained by Ngai and Strom [2] using the FE model to the n(T) values we obtain here employing the CPE.

We first tried fitting to the circuit of Fig. 2(a), where $C_\infty \equiv \varepsilon_B C_0$ is the high-frequency limiting bulk capacitance, involving the bulk dielectric constant ε_B. Considerable fitting attempts using this circuit established that G_s could not be reliably estimated using any of the present data. Therefore, we have used the circuit of Fig. 2(b) for all fitting runs. This circuit combines features of the high-temperature circuit used earlier for the present material [6] and that used for all the present data by Bruce *et al.* [9]. It involves two CPE's, one with A_{0I} and n_I to represent interface effects for the present situation with blocking electrodes, and one involving A_{0B} and n_B to take account of bulk effects. For non-blocking electrodes, one could take $A_{0I} \to \infty$ to eliminate this element. When A_{0B} is taken zero, so $(CPE)_B$ is eliminated, one obtains the high-T circuit [6], while when A_{0I} is taken infinite, one obtains the Bruce *et al.* circuit [9]. Although the earlier analyses [9,10] of the present blocking-electrode data used this circuit with no $(CPE)_I$, and did not employ complex least-squares fitting, the effects of $(CPE)_I$ indeed prove to be nearly negligible over the available data frequency range for the lower-temperature data sets. But we have found that $(CPE)_I$ is necessary to allow good fits to the lower-frequency parts of the data for T > 121 K. Its presence leads to dominant ω^{-n_I} response in the total Z^* of the circuit for sufficiently low frequencies. Further, as we shall see, the inclusion of $(CPE)_I$ somewhat modifies the fitting results obtained for the

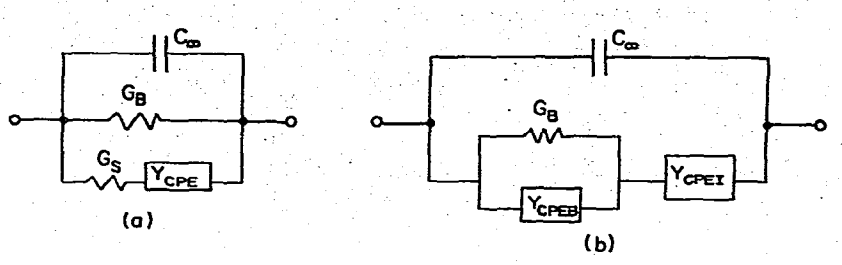

Fig. 2. Two possible fitting circuits for the present data.

other parameters, even at temperatures as low as 102 K. Thus, both CPE's are required, at least in an intermediate temperature range. We have included both in our least squares fitting whenever all their parameters could be well estimated from the fitting procedure. In addition, when appropriate and needed, we have included fixed parameter values outside this full-fit range which were obtained from extrapolation of corresponding parameter values within the full-fit range.

Graphic fitting results

Three-dimensional perspective plots of Z^*, Y, M, and ε data and fitting results and their log-transformation 3-D plots show different aspects of the data and the adequacy of fit because of the different weightings of the various functions. Although space limitations preclude our presenting many of these possibilities, we do include in Fig. 3 regular and log 3-D plots involving fits to the Fig. 2(b) circuit for the three representative temperatures 83, 113, and 151 K. In all these figures, the predicted curves and their vertical projection lines to the bottom plane are given by dotted lines. Generally, the data fits are very good for the lower temperatures and become worse as T increases beyond 113 K. Note that because of the use of P-weighting, we expect and find that the relative fit is as good in regions where a given quantity is very large as it is in regions where the quantity is very small. The fits obtained here are very much better than those shown by Ngai and Strom [3] of M'' *vs* log(ν) for 92 and 102 K, where their predicted M'' values lie quite far below the data lines at frequencies beyond the maximum in M''. These authors ascribe this disagreement to the possible presence of tunneling modes not included in their model. Alternatively, it may arise from the necessarily approximate fitting procedure they used. Thus,

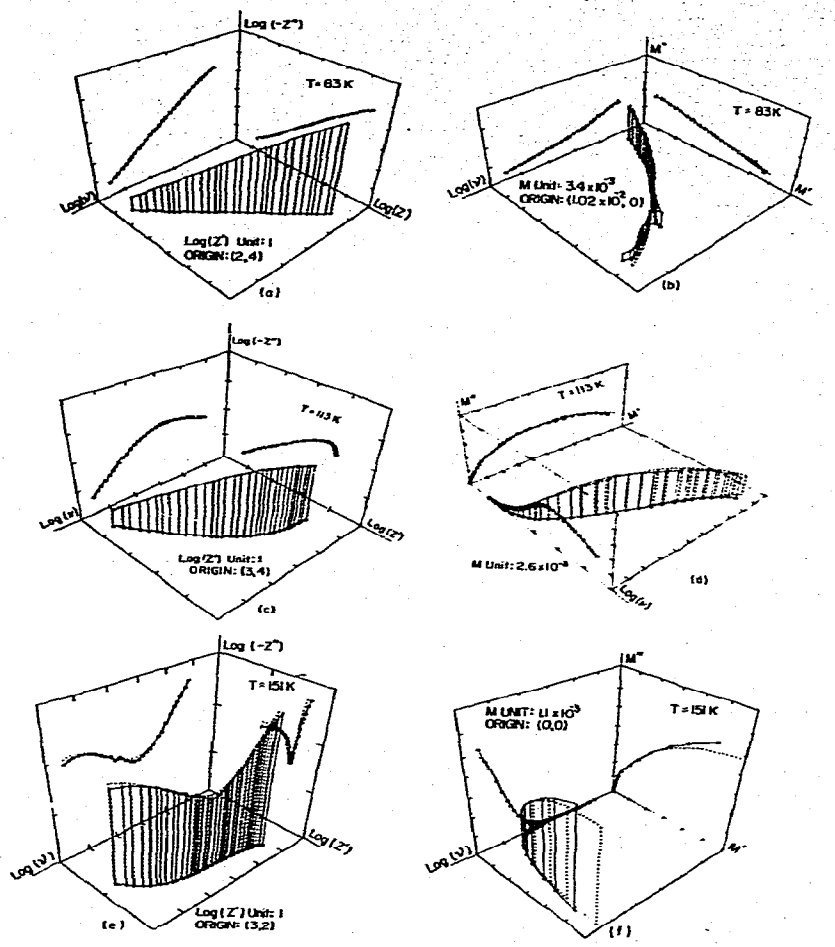

Fig. 3. Three-dimensional perspective plots showing data and fitting results for (a), (b) T = 83 K; (c), (d) T = 113 K; and (e), (f) T = 151 K.

it is not yet clear whether the FE model can yield fits to these data as good (or better) than those obtained here employing the Fig. 2(b) circuit, which only involves a single significant CPE at these temperatures.

DATA ANALYSIS AND RESULTS

Parameter results

Estimates of the following quantities were usually obtained from complex

least-squares fitting of the impedance data: C_∞, G_B, A_{oB}, n_B. At the higher temperatures, we were sometimes able to estimate A_{oI} and n_I as well. From the conductance value, we may directly calculate the conventional quantity $\sigma T \equiv gTG_B$, where g is the cell constant. This identification requires that $n_B(T)$ be greater than zero and assumes that there are no further dispersion regions below the lowest frequencies measured. Figure 4 presents semilog plots of $n_B(T)$ and $C_\infty(T)$ *vs* $10^3/T$ and also a linear graph comparing two other sets of n_B estimates [2,10]. The standard deviation estimates following from the least-squares fit are shown when they are large enough to be distinguished. It proved impossible to obtain least-squares fits at $T > 132$ K when A_{oB} and all other parameters were free to vary. This was probably because the data were not sufficiently accurate, or because they did not extend to sufficiently high frequencies, or because the model was slightly inaccurate. It was found possible, however, to obtain good fits when A_{oB} values were fixed. Therefore, for the fits at the higher temperatures, fixed values of A_{oB} obtained from extrapolation from the lower temperature data were employed, and n_B, G_B, A_{oI}, C_∞, and n_I were taken free to vary. Further, n_I was found to be essentially unity for $T < 151$ K and was taken fixed at this value for lower temperatures. Those A_{oB} points marked with crosses in the figures are extrapolated results. We believe that the extrapolated and fitted values of the parameters for the higher temperatures, while significantly less accurate than those obtained with all parameters free, are still sufficiently accurate to be useful.

One of the most surprising features of the plots is the clear offset and break in the results between T = 102 and 110 K. This is consistent with the presence of a glass-like transition such as that found in polymers [27] from a rubber-like behavior above the glass transition temperature T_g to a glass-like behavior below T_g. No such clear break or division of results into two different temperature regimes was found by Almond *et al.*[10] in their appreciably less accurate analysis of the present data. As already mentioned, however, Ngai and Strom [2,3] have collected much evidence for the existence of a glass-like transition in Na β-alumina with T_g around 120 to 125 K. They particularly demonstrate non-monotonic behavior in their n(T) parameter below 113 K, as their replotted results for n in Fig. 4(b) show. Although it seems quite clear from the results of Fig. 4(a) that the present $n_B(T)$ is well fitted on either side of the break by an equation of the form $n_B(T) = n_{B\infty}\exp(\Delta H_n/kT)$, where $n_{B\infty}$ is temperature independent and ΔH_n is an enthalpy associated with n_B, it is obvious from Fig. 4(b) that $n_B(T)$ may also be quite well fitted by linear relations, and that the present n_B results differ very appreciably from with those obtained by Ngai and Strom [2] and Almond *et al.* [10]. We must again caution, however, that the Ngai-Strom n's are not entirely equivalent to the others and are quite approximate. Here lines have

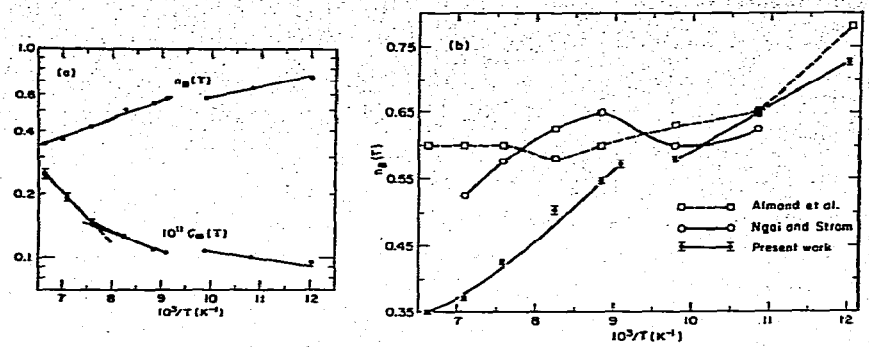

Fig. 4. Data fitting results for $10^{11}C_\infty$, with C_∞ in farads, and for $n_B(T)$, all *vs* $10^3/T$. (a) Semilog plots; (b) linear plots.

been drawn between points to guide the eye. Although there are strong differences apparent among the three dependences, the present results and those of Ngai and Strom certainly show the possibility of a conduction anomaly between 102 and 113 K.

Figure 5 shows semilog results for σT, A_{oB}, A_{oI}, and ν_p *vs* $10^3/T$. The ν_p results will be discussed later. The σT and A_{oB} points show good adherence to simple thermally activated behavior in two temperature ranges separated by clear breaks and offsets. At 151 K, we found $n_I \cong 0.914 \pm 0.021$ and $A_{oI} \cong (3.98 \pm 0.68) \times 10^{-8}$. A least-squares estimate of A_{oI} could not be obtained much below 132 K, but the results of Fig. 5(a) show that it appears to approach a saturation value of $A_{oIC} = 1.6 \times 10^{-8}$ at lower temperatures. Then A_{oI} is approximately given by A_{oIC} plus a thermally activated part, A_{oIT}, which probably involves a larger activation enthalpy than that for A_{oB}. Since A_{oIT} is negligible compared to A_{oIC} for $T \lesssim 121$K, we have used the fixed value $A_{oI} = A_{oIC}$ for fitting at lower temperatures. Since n_I is taken as unity in this range, A_{oIC} then represents an ordinary capacitor. Its presence (rather than $A_{oI} \to \infty$, which eliminates $(CPE)_I$ effects completely) leads to some significant changes in fitting results at say 113 K, but its effects become progressively less as T decreases and are completely negligible at 83 K. Likewise, the effects of $A_{oB} > 0$ become progressively smaller for $T > 121$ K.

Analysis

How can we interpret the apparent limiting capacitance $C_{oIC} = A_{oIC} = 1.6 \times 10^{-8}$ F found in the last section? First, it presumably represents the result of two interface capacitances in series, one at each electrode and here assumed equal. Second, assume that they involve $\varepsilon_B = C_\infty/C_o$, which is found to be about 31 at 113 K, using the C_∞ fitting result for this temperature and assuming, in spite of its appreciable temperature dependence, that C_∞

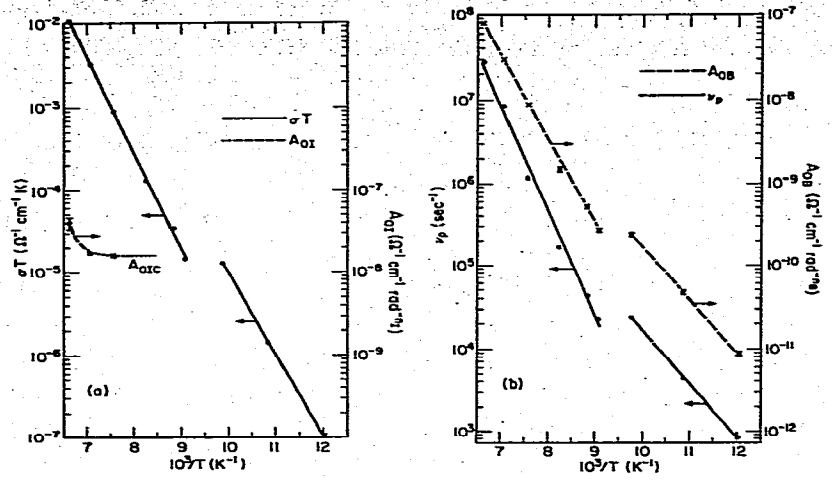

Fig. 5. Data fitting results for (a) σT and A_{OI}, and (b) A_{OB}, and derived results for ν_p, all *vs* $10^3/T$.

represents the bulk capacitance of the material. This dielectric constant value, though it seems rather high, is not necessarily inconsistent with values of 20 to 25 obtained from room-temperature microwave measurements on Na β-alumina [28]. If $2C_{OIC}$ is assumed to arise from a charge-free region of thickness ℓ_c and dielectric constant 31, one obtains $\ell_c \approx 1.3 \times 10^{-5}$ cm, somewhat thicker than seems likely. Alternatively, if $2C_{OIC}$ is taken as a diffuse double layer capacitance involving the Debye length L_D, one can calculate that the necessary ionic concentration to yield 3.2×10^{-8} F is about 10^{15} cm^{-3}, far less than the likely bulk ionic concentration at this temperature. This is only plausible if one assumes the presence of a disturbed region of the material near the electrodes, a region where the concentration of mobile Na ions is greatly depleted. Further, it appears that any intrinsic potential difference between a gold electrode and the bulk of the material would be too small to produce an exhaustion-depletion region of the required thickness. Even a potential difference of 4 eV would lead to a bulk concentration value of only about 4×10^{17} cm^{-3}, still several orders of magnitude too small.

Next, let us begin to consider the dependences and possible inter-relations of the other parameters estimated from the fittings at the nine different temperatures. First consider some of the limiting behavior of the Fig. 2(b) circuit, whose total admittance is $Y_T \equiv Y_T' + iY_T'' \equiv Z_T^{-1}$. We take $Y_{CPEB} \equiv A_{oB}(i\omega)^{n_B}$ and $Y_{CPEI} \equiv A_{oI}(i\omega)^{n_I}$. Let $R_B \equiv G_B^{-1}$. Then, for $\omega << (G_B/A_{oB})^{1/n_B}$:

$$Z_T \rightarrow R_B + A_{oI}^{-1}\,[\cos(n_I\pi/2) - i\sin(n_I\pi/2)]\omega^{-n_I} \tag{2}$$

while for $\omega >> (G_B/A_{oI})^{1/n_I}$:

$$Y_T \rightarrow i\omega C_\infty + G_B + A_{oB}[\cos(n_B\pi/2) + i\sin(n_B\pi/2)]\omega^{n_B} \tag{3}$$

This last result leads to:

$$\sigma_{ac}(\omega) \equiv g\mathrm{Re}[Y_T(\omega)] \cong g[G_B + A_{cB}\,\omega^{n_B}] \tag{4}$$

where

$$A_{cB} \equiv A_{oB}\cos(n_B\pi/2) \tag{5}$$

As Jonscher [29] has pointed out, it has long been known that many amorphous and hopping materials exhibit AC conductivity response of the form:

$$\sigma_{ac}(\omega) = \sigma(0) + B(T)\omega^{n(T)} \tag{6}$$

with $0 < n(T) < 1$, where n(T) has been interpreted by Pollak and Geballe [30] as associated with a distribution of hopping probabilities between sites distributed randomly in space and energy. Since equations (4) and (6) are equivalent if we take $n = n_B$, the AC conductivity of the Fig. 2(b) circuit agrees with the equation (6) prediction as long as $\omega >> (G_B/A_{oI})^{1/n_I}$. Now, Almond *et al.*[10] have written a relation proposed by Jonscher for hopping conduction [31] for the imaginary part of the dielectric permittivity, χ'', in the following form:

$$\sigma_{ac}(\omega) \equiv \varepsilon_0\omega\chi''(\omega) = K_a\nu_p + K_a\nu_p^{1-n_B}\,\omega^{n_B} \tag{7}$$

where they initially take K_a as a constant. Note that this result, if applicable, immediately establishes a relation between $\sigma(0) \equiv \sigma$ and B(T). Here:

$$\nu_p \equiv \nu_o\exp[\Delta S_p/k]\exp[-\Delta H_p/kT] \equiv \nu_e\exp[-\Delta H_p/kT] \tag{8}$$

where ν_p is the hopping frequency of ions, ν_0 is the hopping attempt frequency, and ΔS_p and ΔH_p are the entropy and enthalpy of hopping.

Almond *et al.* [32] have applied equation (7) to data on four widely differing structures, including Na β-alumina [10,32]. They introduce the following expression for K_a given by Huggins [33] and derived from random walk theory applied to $\sigma(0)$:

$$K_a = \alpha\beta a^2 c_0 e^2/kT \equiv K_0(T)/T \tag{9}$$

Here, we have introduced the new function $K_0(T)$, proportional to βc_0. In the above equation α is a geometric factor involving the number of possible jump directions from a given site; it is 1/4 for the two-dimensional ionic motion most appropriate for Na β-alumina. The quantity, a, is the hopping distance; e is the proton charge; and k is Boltzmann's constant. The parameter β is defined by Huggins as the fraction of the species that is free to move, and c_0 is the concentration of mobile species, here Na ions. Let us define N_0 as the stoichiometric concentration of Na ions, and $N_x \equiv (1 + x)N_0$, where N_x is the maximum concentration of ions. If we assume as usual [4] that the N_0 ions are in deep-well Beevers-Ross positions in the lattice and contribute little to the conductivity, then $c_{omax} \cong N_x - N_0 = xN_0$. Define $c_0/c_{omax} \equiv \delta(T)$. Then since β measures the fraction of empty sites for ions, we may write $c_0\beta = c_{omax}\,(c_0/c_{omax})[1 - (c_{omax}/N_0)] = N_0 x\delta(1 - x)$. A somewhat similar but non-equivalent expression has been given by Almond *et al.* [10,32]. Now, equations (6), (7) and (9) lead to $\sigma(0) \equiv \sigma = K_a\nu_p \propto c_0\beta$. When $c_0 \cong c_{omax}$, we see that the above result for $c_0\beta$ yields $\sigma \propto x(1-x)$. It is worth noting that Dudley and Steele [34] have found evidence for $x(1 - x)$ behavior in $K_{1+x}Fe_{11}O_{17}$ with x variable over a wide range. We may now write:

$$K_0(T) \equiv K_{00} x\delta(1 - x) \tag{10}$$

where $K_{00} \equiv \alpha a^2 e^2 N_0/k$, is taken to be temperature independent. Note that setting equations (4) and (7) equal leads to the relations $gG_\beta = K_a\nu_p$ and $gA_{cB} = K_a\nu_p^{1-n_B}$. In turn these results immediately yield:

$$\nu_p = (G_\beta/A_{cB})^{1/n_B} \tag{11}$$

and

$$K_0(T) = gT(A_{cB}G_\beta^{n_B-1})^{1/n_B} \tag{12}$$

These expressions may be used with estimated values of G_B, A_{oB}, and n_B to test the validity of equations (7), (8) and (10) for specific data and to find estimates of $K_o(T)$, K_{oo} and $\delta(T)$.

Although Almond *et al.* [10,32] mentioned the possibility of thermal activation of c_o, they did not introduce such dependence in most of their analyses. Here we propose to do so and, in addition, to consider the possibility of a glass-like transition in Na β-alumina. Wolf [35] has given a complex theory of conduction in Na β-alumina which involves clustering of ions, motion between several non-equivalent sites, and thermal activation of carriers. This theory involves more parameters than we can adequately determine from the present data. Thus, we shall use the simple hopping theory leading to equation (9) and consider simplified average motion with a single average hopping distance. Materials which undergo a glass transition are generally well described above T_g by the Vogel [36]-Fulcher [37] equation:

$$\tau = \tau_o \exp[\chi/(T - T_\infty)] \tag{13}$$

where τ is a relaxation rate, χ is temperature independent, and T_∞ is the Vogel temperature, generally [38] 20 to 100 degrees below T_g. At the Vogel temperature the viscosity of the material would become infinite, but this equation is usually applied [27] only above T_g. Zeller [39] has, however, shown that it applies in some materials below T_g but still above T_∞. It has also been shown [38] that equation (13) is fully consistent with and equivalent to the well-known empirical Williams-Landel-Ferry (WLF) [27] equation.

In the present situation, there seem to be only two basic quantities which might possibly involve $(T-T_\infty)$ behavior near the glass-like transition: the concentration of charge carriers and the hopping frequency. Figure 5(b) shows results for $\nu_p(T)$ calculated from equation (11) using estimated parameter values obtained from the least-squares data fitting. We see that $\nu_p(T)$ is well thermally activated in the lower temperature regions and at least approximately so for the upper one; the pertinent parameters are listed in Table 1 and will be discussed further below. Therefore, the data rule against a $(T-T_\infty)$ dependence of ν_p. Indeed, for $T < T_\infty$, a dependence of the form $\nu_p = \nu_e \exp[-\chi/|T-T_\infty|]$ would lead to ν_p increasing rather than decreasing with temperature. Even for $T > T_\infty$, this expression for ν_p yields a far worse fit of the data with $T_\infty > 0$ than with $T_\infty = 0$ (ordinary thermal activation). But the situation may be different for the ionic concentration. Suppose that $\delta = \exp[-\chi/|T-T_\infty|]$. Again we must take $T_\infty = 0$ in this formula for the $T < T_\infty$ region since δ should decrease, not increase, as T drops. But a value of $T_\infty > 0$ in the above expression when $T > T_\infty$ may not be precluded by the data. The results of Figs. 4 and 5 already show that something anomalous occurs between

T = 102 and 110 K. Thus, it is reasonable to expect that if indeed $T_\infty > 0$ for c_0 dependence, it will fall in this range. The assumption of $T_\infty > 0$ for the higher-temperature data is quite speculative, and the results must be evaluated by their internal consistency, their agreement with known parameter values for Na β-alumina, and their predicted value. Note that the temperature dependence of $K_0(T)$, whatever it is, doesn't directly influence $\nu_p(T)$ values calculated using equation (11). When $T_\infty = 0$, we may identify χ as $\Delta H_p/k$. But when $T_\infty > 0$, χ is not related to a thermal activation enthalpy but is just a temperature-independent constant, part of the temperature-dependent free energy of the carrier activation process [38]. Clearly the presence of $T_\infty > 0$ yields zero conductivity at $T = T_\infty$! Although for real materials it is not likely that the Vogel-Fulcher equation would apply exactly down to $T = T_\infty$, even if it applied approximately in the region near T_∞, one would expect to see some extra decrease in σ in this neighborhood. Some such behavior does seem to appear at 110 K for the σ(T)T curve of Fig. 5, and it should show up much clearer, if present, in a $K_0(T)$ curve calculated with equation (12).

Thermal activation and other equation fitting results

Table 1 presents activation parameters derived from the fitting results for each of the five quantities σT, A_{0B}, C_∞, n_B, and ν_p for the higher, then the lower temperature region. It is not clear why C_∞ and n_B show good thermal activation. Most theories that involve an n exponent, such as the infrared divergence response model of Ngai and Strom [2], do not yield a micro- or even macroscopic basis for temperature dependence of n. A treatment involving distributions of pre-exponential factors and activation energies [40] does yield a quantity equivalent to n_B for t^{-n} response, but its temperature dependence is not of exponential form. Because of our use of extrapolated A_{0B} values above T = 121 K, results for increasing higher temperatures become more and more uncertain, and even results for this temperature are not very consistent with those below it, as shown by the values presented in Fig. 4 and 5. It seems especially likely that the large increases in C_∞ above 121 K arise from the use of inaccurate fixed values of A_{0B} for the three highest temperatures. The C_∞ results in the Table were thus calculated using only 110 K ≤ T ≤ 132 K values and T = 92 and 102 K values. Similarly, the low-T n_B results were calculated using only these two temperatures. Because of the uncertainty in the 121 K A_{0B} value, the high-T A_{0B}-related values in the Table and the extrapolated results were obtained using only T = 110 and 113 K fitting values. It may be significant that several high-T ΔH's are about twice the corresponding low-T ΔH.

All the least-squares results summarized in Table 1 were obtained using nonlinear least-squares fitting with P-weighting rather than linear fitting of the

TABLE 1

Calculated activation-type quantities of the form $Q = Q_\infty \exp[-\eta/T] \equiv Q_\infty \exp[-\Delta H_Q/kT]$. The first line of each pair applies for $T > 110$K and the second for $T < 102$K.

Quantity Q	Q_∞	η (K)	ΔH_Q (eV)
σT ($\Omega^{-1}cm^{-1}K$)	5.00×10^5	2663	0.229
	2.54×10^4	2181	0.188
A_{oB} ($\Omega^{-1}cm^{-1}rad^{-n_B}$)	5.51×10^1	2868	0.247
	4.66×10^{-4}	1477	0.127
C_∞ (farads)	7.80×10^{-12}	221	0.019
	2.14×10^{-12}	70	0.006
n_B	8.61×10^{-2}	-210	-0.018
	2.19×10^{-1}	-99	-0.009
$\nu_p(s^{-1})$	7.05×10^{15}	2940	0.253
	6.82×10^{10}	1520	0.131

log-transformed exponential equation for thermal activation. The results also yielded estimates of the standard deviations of the parameter values shown in the Table. Because of irregularities in the points fitted, standard deviations for a few Q_∞ values were as large as Q_∞ itself, indicating that the pre-exponential coefficient was not adequately determined by the data. In all cases, its relative error was much larger than that for η. The best results were those for $T < 102$ K, although those for σT for $T > 110$ K were also good.

The ν_p results in Fig. 5(b) were calculated using equation (11) and thus reflect possible errors in the fitting estimates of G_B, A_{oB}, and n_B. Because of correlation between various quantities, it is impractical to try to estimate closely the standard deviations of the ν_p calculated values. But the uncertainty in ν_p (and K_o) values is here dominated by uncertainty in n_B. For example, if we use the $T = 113$ K n_B estimate, $n_B \pm \sigma_n = 0.547 \pm 0.004$, and calculate ν_p for this temperature with $n_B + \sigma_n$, n_B, and $n_B - \sigma_n$, we find $\nu_p = (4.39 \times 10^4 \pm 2.8 \times 10^3)\ s^{-1}$, enough variation to put this point on the best-fit line and probably a lower estimate at that. A single σ_n change as above, or even less a change, would make all the high-T ν_p points fall on a straight line. With these caveats about accuracy, we can conclude that ν_p values calculated using equation (11) are consistent with equation (8), apparently

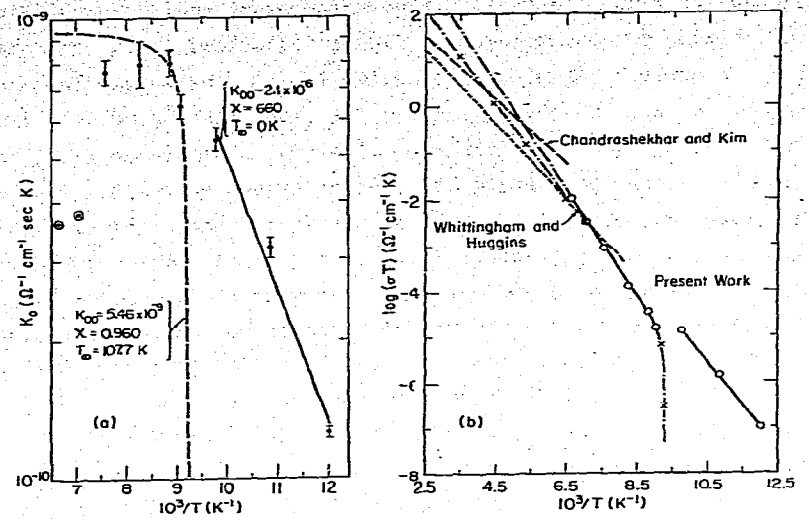

Fig. 6. (a) Calculated and fitted results for $K_0(T)$, and (b) various results for $\log(\sigma T)$ *vs* $10^3/T$.

justifying equation (7). But the $T < 102$ K value found for ν_e is $(6.82 \times 10^{10} \pm 3.57 \times 10^{10})$ s^{-1}, appreciably smaller than the expected value [10,32] of $\nu_o \approx 2 \times 10^{12}$ Hz obtained directly from infrared absorption measurements [41]. It appears that ν_o is indeed nearly temperature independent in the present range of temperatures [41]. If this value of ν_o is accepted, one requires a value of $\Delta S_p/k$ of about -3.4! Although negative entropy values have been invoked in some dielectric measurements [42], the necessity of such a value here casts some doubt on the applicability of equation (7), at least below the transition-break region.

The situation is somewhat brighter for the $T > 110$ K results. Here $\nu_e = (7.1 \times 10^{15} \pm 8.3 \times 10^{15})$ s^{-1}, leading to $\Delta S_p/k = 8.2$, rather larger than one might expect. But this obviously uncertain value of ν_e is derived from all the ν_p values for $T > 110$ K, including the quite uncertain higher temperature estimates. When only ν_p values for $T = 110$, 113, and 121 K are used, one obtains $\nu_e = (5.49 \times 10^{13} \pm 4.65 \times 10^{13})$ s^{-1} and $n_p = (2376 \pm 97)$. This again uncertain estimate of ν_e leads to $\Delta S_p/k = 3.3$, a more reasonable value. If we try fitting these three ν_p points with ν_e fixed at 2×10^{12} s^{-1}, we obtain $n_p = (1999 \pm 11)$, but the standard error of fit is about three times worse. These

results certainly do not allow us to reject equation (7), but neither do they confirm it strongly.

One might hope that K_0 values calculated using equation (12) would yield further justification for equation (7). Figure 6(a) shows our K_0 results with minimum likely error bars calculated using $(n_B \pm \sigma_n)$. Now what value might we expect for K_{00}? For N_x, we take (1 + x)(2 layers/unit cell)/(volume of unit cell), yielding 4.018×10^{21} cm^{-3} for x = 0.227 [4]. This value of N_x is stated by Wang [4] to be the average Na^+ concentration, but he was considering higher temperatures and essentially full activation of the carriers. The corresponding value of c_{omax} is about 7.4×10^{20} cm^{-3} for this value of x, much larger than that estimated from A_{0IC}. Then with a = d = 5.594 A, the lattice parameter in the c-plane and the distance between Beevers-Ross and anti-Beevers-Ross positions, we obtain $K_{00} = 4.76 \times 10^{-9}$ (Ω^{-1} cm^{-1} s K). Clearly, the value of 2.1×10^{-6} found from the least squares exponential fit for T < 102 K is wholly inconsistent with this value. But if we ignore the 83 K value, assume $\delta = 1$, and average the other two values, we obtain $K_{00} = 2.5 \times 10^{-9}$, fairly close. The verdict must again be suggestive but not proven.

The T > 110 K dashed curve in Fig. 6(a) was obtained from fitting of equation (10) with δ as given above and T_∞ a free parameter. The exact estimates of K_0 at T = 110 and 113 K were used along with the T = 121 K value plus its estimated standard deviation. The fitting equation does not allow a decrease in K_0 to occur as the temperature increases. Although we let K_{00}, x, and T_∞ be free in this fitting, data were insufficient to allow us to take x free as well, and it was held fixed at 0.227. The availability of more points of higher x accuracy would, however, allow it to be estimated also. We have ignored the very uncertain higher temperature K_0 points, especially the T = 141 and 151 K estimates shown with circles. We see that the value of K_{00} obtained from this fit, 5.46×10^{-9}, is quite close to the value calculated above and the T_∞ estimate is also plausible. But an average of the four K_0 values from T = 110 to 132 K yields $K_{00} = 4.29 \times 10^{-9}$ if we assume $\delta = 1$ at all these temperatures. This result is even closer to the calculated value. We can certainly conclude from these results that either of the last two calculated K_{00} values strongly justifies the applicability of equations (7) through (12) for T > 110 K. But the uncertainties in the K_0 data do not allow us to conclude unambiguously that δ obeys a Vogel-Fulcher type of equation with $T_\infty = 108$ K. If the T = 113 and 110 K K_0 points are to be trusted, $c_0 \cong c_{omax}$ for T > 130 K, and c_0 decreases very rapidly as T drops from 110 K towards T_∞. Thus, we can only conclude that Vogel-Fulcher behavior cannot be ruled out by the present data. More accurate impedance-frequency data in the region between 102 and 110 K would certainly allow much further clarification of the matter, including how the low and high temperature lines join up.

Figure 6(b) presents σT results over a much wider temperature range. The dotted and dashed lines show the higher-temperature results of Whittingham and Huggins [1] and of Chandrashekhar and Kim [7]. Our present σT results are also shown with an extrapolation to higher temperatures based on the full σT data fit. It clearly lies higher than likely at high temperatures. Alternatively, the crosses show extrapolations at both ends, using $T\sigma = K_o(T)\nu_p$, based on the Vogel-Fulcher K_o-fit results along with the ν_p parameters obtained from the temperatures 110, 113, and 121 K. Note that, direct extrapolation of the $T < 102$ K results would yield a line quite close to that of Whittingham and Huggins. Of course, the possible approach toward zero as $T \to T_\infty$ shown here is quite speculative and needs further investigation with more and much better data.

CONCLUSIONS

We have demonstrated how 3-D perspective plotting of impedance data on Na β-alumina, and complex non-linear least-squares analysis of the data, may be used to discover and emphasize problems and effects not apparent with other less powerful methods having smaller resolving power [8,9,32]. Fitting of the data to an appropriate equivalent circuit showed a clear break and offset in the thermal activation lines of all significant circuit and derived parameters. The break fell between the lines for 110 K and up and those from 102 K downwards. Analysis of parameter estimates derived from fitting suggested the presence of a glass-like transition affecting the conductivity of the material and occurring above the Vogel temperature, T_∞, estimated as falling at about 108 K. The results of the data analysis further strongly suggested that for $T > T_\infty$ there is a direct connection between the low-frequency limiting conductivity of the material and the Na-ion hopping rate. Good agreement was found between a value of a conductivity pre-exponential factor, K_o, calculated from the fitting results and a value calculated directly from simple random walk theory. It thus appears, as first suggested by Almond *et al.* [32] that AC measurements may be used to estimate both the DC conductivity and the ionic hopping rate for this and possibly some other solid materials, even when ionically blocking electrodes are employed.

ACKNOWLEDGEMENTS

We much appreciate the helpful suggestions of Drs. Sang-Il Choi, S. W. Kenkel and J. C. Wang. We are grateful to the U.S. Army Research Office for support.

REFERENCES

1 M.S. Whittingham and R.A. Higgins, J. Chem. Phys., 54 (1971) 414-416.
2 K.L. Ngai and U. Strom, Phys. Rev., B27 (1983) 6031-6036.
3 U. Strom, Sol. State Ionics, 8 (1983) 255-279.
4 J.C. Wang, Phys. Rev., B27 (1983) 6088-6096.
5 K.K. Kim, J.N. Mundy and W.K. Chen, J. Phys. Chem. Solids, 40 (1979) 743-755.
6 H. Engstrom, J.B. Bates and J.C. Wang, Solid State Commun., 35 (1980) 543-546.
7 G.V. Chandrashekhar and K.K. Kim, Solid State Commun., 37 (1981) 299-301.
8 D.P. Almond and A.R. West, Solid State Ionics, 3/4 (1981) 73-74.
9 P.G. Bruce, A.R. West and D.P. Almond, Solid State Ionics, 7 (1982) 57-60.
10 D.P. Almond, A.R. West and R.J. Grant, Solid State Commun., 44 (1982) 1277-1280.
11 J.R. Macdonald, J. Schoonman and A.P. Lehnen, J. Electroanal. Chem., 131 (1982) 77-95.
12 J.R. Macdonald, J. Schoonman and A.P. Lehnen, Solid State Ionics, 5 (1981) 137-140.
13 G. Williams and D.C. Watts, Trans. Faraday Soc., 66 (1970) 80-85.
14 K.L. Ngai, Comments Solid State Phys., 9 (1979) 127-140; 9 (1980) 141-155.
15 C.T. Moynihan, L.P. Boesch and N.L. Laberge, Phys. and Chem. of Glasses, 14 (1973) 122-125; J.H. Ambrus, C.T. Moynihan and P.C. Macedo, J. Phys. Chem., 76 (1972) 3287-3295.
16 A.R. West, private communication.
17 R.J. Grant, M.D. Ingram and A.R. West, Electrochim. Acta, 22 (1977) 729-734.
18 J. Schrama, Thesis, Leiden, (1957) pp. 60-61.
19 K.S. Cole and R.H. Cole, J. Chem. Phys., 9 (1941) 341-351.
20 J.R. Macdonald, in M. Kleitz and J. Dupuy (Eds.), Electrode Processes in Solid State Ionics, Reidel, Dordrecht, Holland, 1976, pp. 149-180.
21 J.R. Macdonald, in G.D. Mahan and W.L. Roth (Eds.), Superionic Conductors, Plenum, New York, 1976, pp. 81-97.
22 W.I. Archer and R.D. Armstrong, Electrochemistry, Chemical Society Specialist Periodical Report, 7 (1980) 157-202.
23 R.P. Buck, Sensors and Actuators, 1 (1981) 137-196.
24 J.R. Macdonald, A. Hooper and A.P. Lehnen, Solid State Ionics, 6 (1982) 65-77.
25 J.R. Macdonald and M.K. Brachman, Rev. Mod. Phys., 28 (1956) 393-422.
26 J.R. Macdonald, submitted to Solid State Ionics.
27 J.D. Ferry, Viscoelastic Properties of Polymers, Wiley, New York, Third Edition, 1980, pp. 274, 280-290.
28 A.S. Barker, J.A. Ditzenberger and J.P. Remeika, Phys. Rev., B14 (1976) 4254-4265.
29 A. K. Jonscher, J. Phys. C: Solid State Phys., 6 (1973) L235-239.
30 M. Pollak and T.H. Geballe, Phys. Rev., 122 (1961) 1742-1753.
31 A.K. Jonscher, Phys. Thin Films, 11 (1980) 232.
32 D.P. Almond, G.K. Duncan and A.R. West, Solid State Ionics, 8 (1983) 159-164.
33 R.A. Huggins, in A.S. Nowick and J.J. Burton (Eds.), Diffusion in Solids, Recent Developments, Academic, London, 1975, pp. 445-486.
34 G.J. Dudley and B.C.H. Steele, J. Solid State Chem., 21 (1977) 1-12.
35 D.J. Wolf, J. Phys. Chem. Solids, 40 (1979) 757-773.
36 H. Vogel, Phys. Z., 22 (1921) 645-646.
37 G.S. Fulcher, J. Am. Ceram. Soc., 8 (1925) 339-355; 789-794.
38 J.R. Macdonald, J. Chem. Phys., 40 (1964) 1792-1804.
39 H.R. Zeller, Phys. Rev. Lett., 48 (1982) 334-337.
40 J.R. Macdonald, J. Appl. Phys., 34 (1963) 538-552.
41 S.J. Allen Jr. and J.P. Remeika, Phys. Rev. Lett., 33 (1974) 1478-1481.
42 K.Higasi, Dielectric Relaxation and Molecular Structure, Kasai Publ. Co., Tokyo, 1961, pp. 12-13.